

Stability and electronic properties of the $\text{LaNiO}_2/\text{SrTiO}_3$ interface

F. Bernardini¹ and A. Cano²

¹*Dipartimento di Fisica, Università di Cagliari, IT-09042 Monserrato, Italy*

²*Institut Néel, CNRS & UGA, 38042 Grenoble, France*

(Dated: December 3, 2021)

Infinite-layer nickelate thin films materialize an intriguing new platform for high-temperature unconventional superconductivity, with $\text{LaNiO}_2/\text{SrTiO}_3$ as reference setup. We discuss the relative stability of the elementary interfaces of this system and determine the corresponding electronic band structure. We find substantial changes compared to the bulk, in particular in relation to the $5d$ orbital contributions to the low-energy physics which can be totally replaced by purely $\text{Ni-}3d$ flat bands. The d^9 configuration characteristic of cuprates can thus be supplemented by an extra interfacial ingredient destabilizing the normal non-superconducting state in these heterostructures.

Infinite-layer nickelates have long been proposed as intriguing analogues to high- T_c superconducting cuprates, thus sustaining a rather fundamental research on these systems over the years [1–6]. This is motivated by the nominal $3d^9$ electronic configuration featured by the Ni and Cu atoms in both these systems, which is however accompanied by a self-doping effect due to rare-earth $5d$ states in the case of the nickelates. As a result of such a “niche” background activity, superconductivity has recently been reported in Sr-doped $\text{NdNiO}_2/\text{SrTiO}_3$ thin films [7]. This finding represents an important breakthrough that, however, seems to be remarkably difficult to reproduce. In fact, the reported T_c ’s vary quite substantially from sample to sample—even if they are nominally equivalent—and no definitive result is given for the $\text{LaNiO}_2/\text{SrTiO}_3$ case [7]. Beyond that, no superconductivity has been found in epitaxial thin films directly grown on SrTiO_3 and alternative substrates and, very importantly, in bulk samples so far [8, 9]. This state of affairs calls for the investigation of the corresponding interface itself since it can play a non-trivial role in the reported superconductivity.

Here, we investigate theoretically the fundamental properties of the reference $\text{LaNiO}_2/\text{SrTiO}_3$ interface by means of density functional theory (DFT) calculations. This system is expected to be representative for the infinite-layer nickelate series without requiring any ambiguous treatment of $4f$ electrons [2, 3, 10–13]. In addition, the DFT band structure near the Fermi level has proven to be rather robust with respect to many-body correlation effects in bulk LaNiO_2 [14]. We model the interface by a symmetric supercell with two identical interfacial layers among the four elementary possibilities illustrated in Fig. 1. Our model is also fully relevant for the ultrathin limit of these systems, as one full LaNiO_2 layer is always sandwiched between the interfaces. Thus, we determine the most stable interfacial configuration according to the corresponding thermodynamics. As we show below, the fragile stability of the infinite-layer bulk nickelates manifests also through the marked differences in the relative energetics of the heterostructure. Thus, the growth process can be expected to have a non-negligible impact on the eventual atomic

configuration that is realized experimentally. In addition, we study the specific features that emerge in the local band structure as a function of such an atomic configuration. We find drastic changes compared to the bulk. In particular, while the $\text{Ni-}3d_{x^2-y^2}$ low-energy features are robust against interfacial effects, the metallic character provided by the $\text{La-}5d$ states in the bulk can be replaced either by $\text{Ti-}3d$ contributions or directly by $\text{Ni-}3d_{z^2}$ flat bands in the ultrathin limit. This modifies qualitatively the initial picture for the development of strong correlations and the eventual Cooper pairing, which then might display a distinct interfacial nature in infinite-layer nickelates of this class.

I. COMPUTATIONAL METHODS

We performed density functional theory (DFT) calculations to investigate the $\text{LaNiO}_2/\text{SrTiO}_3$ heterostructure. We considered a tetragonal supercell with 3 Ni and 3 Ti atoms and two identical boundary layers, simulating the epitaxial LaNiO_2 by imposing the calculated $a = b = 3.94$ Å lattice parameters of bulk SrTiO_3 . The c parameter and the internal atomic positions, in their turn, were optimized using a constrained variable-cell dynamics. In this way, we avoid the presence of the residual stresses that might falsify the relative stability of the different interfacial configurations. We used the VASP code [15] for these calculations with the PBE [16] exchange-correlation functional and PAW pseudo-potentials [17]. We employed a plane-wave cutoff of 540 eV and a Monkhorst-Pack $6 \times 6 \times 2$ k -mesh with a 0.2 eV Gaussian smearing, and treated the $\text{Sr-}4s4p$, $\text{Ti-}3s3p$ and $\text{Ni-}3p$ electrons as valence electrons. The convergence criteria were 1 meV on the total energy, 0.001 Å on the c parameter, and 0.01 eV/Å on the residual forces. The structural parameters of the supercells are summarized in Table I. The corresponding chemical potentials are determined from analogous total energy calculations of equilibrium bulk structures using the same plane-wave cutoff and smearing, and a k -mesh equivalent to a cubic $6 \times 6 \times 6$ one whenever possible. The results are summarized in Table II in the Supplemental Material.

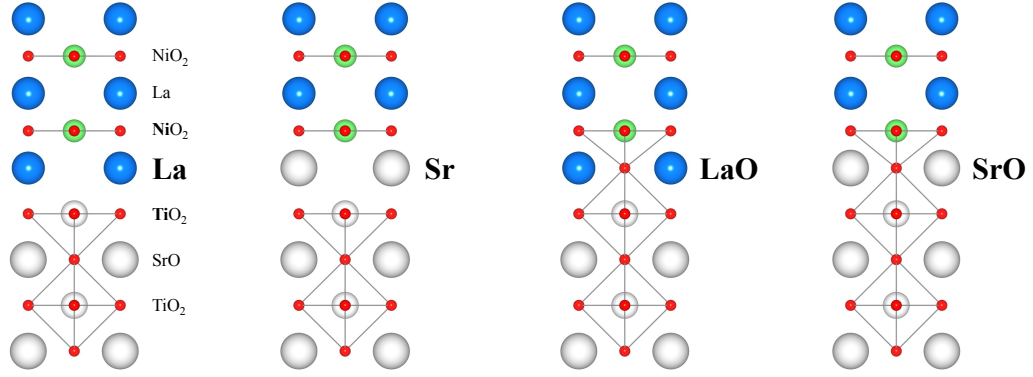


FIG. 1. Ball-and-stick model of the elementary $\text{LaNiO}_2/\text{SrTiO}_3$ interfaces. The boundary layer can be made of either La, Sr, LaO, or SrO planes as indicated in the figure. The interfacial atoms indicated with bold symbols are denoted by the i subscript in the main text.

	La	Sr	LaO	SrO
c (Å)	21.82	21.89	22.50	22.70
$\text{Ni}_i\text{-O}$ (Å)	1.982	1.970	1.977	1.994
$\text{O}_i\text{-Ni}_i$ (Å)	-	-	2.196	1.966
$\angle \text{O}_i\text{-Ni}_i\text{-O}$ (°)	-	-	85.07	98.95
E_{tot} (eV)	-201.07	-192.92	-218.69	-209.13

TABLE I. Structural parameters and total energy of the supercells used to study the four elementary $\text{LaNiO}_2/\text{SrTiO}_3$ interfaces sketched in Fig. 1. Ni_i denotes the first nickel next to the interfacial layer and O_i the interfacial oxygen (bold symbols in Fig. 1). The reported values correspond to the overall c parameter, $\text{O}_i\text{-Ni}_i$ distance, $\text{Ni}_i\text{-O}$ distance, and $\text{O}_i\text{-Ni}_i\text{-O}$ bond angle.

The electronic band structure was further computed using the full-potential linear augmented plane-wave (FLAPW) method as implemented in the WIEN2K package [18], with the LDA exchange-correlation functional [19]. We performed spinless calculations with muffin-tin radii of 2.5, 2.1, 2.0 and 1.5 Bohr for the La (Sr), Ni, Ti and O atoms respectively and a plane-wave cutoff $R_{\text{MT}}K_{\text{max}} = 7.0$. The integration over the Brillouin zone was performed using a $13 \times 13 \times 2$ k -mesh for the self-consistent calculations, while a denser $36 \times 36 \times 6$ k -mesh was used for the Fermi surface.

II. STRUCTURE OF THE INTERFACE

We first address the question of the actual structure of the $\text{LaNiO}_2/\text{SrTiO}_3$ interface. We assume the ideal case in which the interface is not modified by e.g. oxygen vacancies or topotactic hydrogens [20], and such that no interface reconstruction takes place. The latter indeed seems to be the case according to the scanning transmission electron microscopy (STEM) images reported in [21]. In fact, in (001) oriented SrTiO_3 substrates, ideal SrO and TiO_2 terminated surfaces are the most stable con-

figurations according to first-principles calculations [22] and they regularly are realized experimentally [23]. In addition, the closely related $\text{LaAlO}_3/\text{SrTiO}_3$ system for example displays a well defined LaO flat interface (see e.g. [24, 25]).

In order to determine the relative formation energy of the four $\text{LaNiO}_2/\text{SrTiO}_3$ elementary interfaces (see Fig. 1) we follow the thermodynamic approach described in [26–28]. Thus we define the interface energy as

$$E_{\text{interface}} = \frac{1}{2} \left(E_{\text{tot}} - \sum_{\text{X=La, Sr, Ni, Ti, O}} \mu_{\text{X}} N_{\text{X}} \right), \quad (1)$$

where E_{tot} is the total energy of the corresponding supercell, μ_{X} is the chemical potential of the X element, and N_{X} is the number of X atoms in the supercell. In this way, the energy difference between the La and LaO configurations for example can be written as

$$\begin{aligned} \Delta E_{\text{interface}}^{\text{La-LaO}} &= \frac{1}{2} (E_{\text{tot}}^{(\text{La})} - E_{\text{tot}}^{(\text{LaO})}) + \mu_{\text{O}} \\ &= \frac{1}{2} (E_{\text{tot}}^{(\text{La})} - E_{\text{tot}}^{(\text{LaO})} + E_{\text{tot}}^{\text{O}_2}) + \Delta\mu_{\text{O}}, \end{aligned} \quad (2)$$

and likewise for the rest. Here and hereafter $\Delta\mu_{\text{X}} \leq 0$ denotes the chemical potential of X relative to its value in the most stable elementary phase of X (that is, $2\Delta\mu_{\text{O}} = 2\mu_{\text{O}} - E_{\text{tot}}^{\text{O}_2}$ in the case of $\text{X} = \text{O}$). Thus, the relative stability of the different configurations can be nailed down from these chemical potentials, which can be estimated as detailed in the Supplemental Material. The results, summarized in Fig. 2, are as follows.

The two-step synthesis of the samples performed in [7] starts with the epitaxial growth of the perovskite heterostructure—that is, $\text{LaNiO}_3/\text{SrTiO}_3$ in our case. At this stage, the interfacial configuration of the system restricts to either LaO or SrO. In Fig. 2, the horizontal thick line in blue represents the boundary between these two possibilities. Above (below) this line, the LaO (SrO) configuration minimizes the overall energy of the system. However, in thermodynamic equilibrium, the chemical

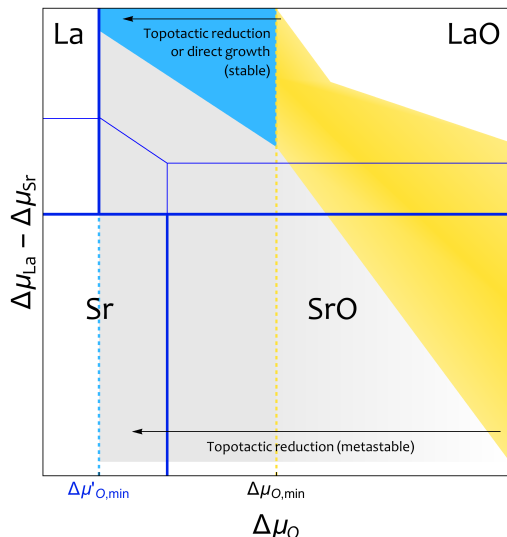


FIG. 2. Calculated phase diagram for the interfacial configuration of the $\text{LaNiO}_n/\text{SrTiO}_3$ heterostructure ($n = 2, 3$). LaO, SrO, La, and Sr label different regions according to the relative stability of the corresponding interfacial configurations (the thin lines apply for the direct growth of $n = 2$). The yellow area indicates the thermodynamically allowed (equilibrium) values of the chemical potentials for $n = 3$, while the blue does for $n = 2$ (as obtained by both topotactic reduction and direct growth). The dashed vertical lines indicate the minimum allowed value of the oxygen chemical potential before and after the topotactic reduction (the dashed blue line also applies for the direct growth for $n = 2$). Both LaO and SrO configurations can be realized in the $\text{LaNiO}_3/\text{SrTiO}_3$ perovskite heterostructure, while only LaO becomes compatible with the stability of the bulk infinite-layer phase in $\text{LaNiO}_2/\text{SrTiO}_3$. The interfacial SrO, Sr (and La) configurations, in contrast, imply the thermodynamic metastability of the system in the latter heterostructure.

potentials have to be inside the yellow region. As a result, the two configurations can be obtained under oxygen-rich conditions while only the LaO one is compatible with the oxygen-poor case ($\Delta\mu_{\text{O}} >$ and < -1.9 eV respectively).

The subsequent topotactic reduction removes oxygens from the nickelate, which in principle enables the additional Sr and La interfacial configurations from the previous ones. This introduces the new LaO-La and SrO-Sr boundaries indicated by the vertical solid lines in Fig. 2. In terms of the chemical potentials, the reduction is associated to the lowering of the minimum allowed value of the oxygen chemical potential $\Delta\mu_{\text{O},\text{min}}$ (from -2.5 eV to -4.4 eV as indicated by the dashed vertical lines in Fig. 2). The La configuration, however, never minimizes the energy above $\Delta\mu'_{\text{O},\text{min}}$ and therefore will not be realized (unless extra oxygen-vacancies be present). The other three configurations are still compatible with the ideal reduction. However, the infinite-layer phase of the bulk nickelate is stable only within the blue region. Consequently, the SrO and Sr configurations can appear but as metastable states of the system, while the LaO configura-

tion is the only one that is in thermodynamic equilibrium with the infinite-layer phase of the bulk nickelate. The analysis of the direct growth of the $\text{LaNiO}_2/\text{SrTiO}_3$ heterostructure yields the same result (with the LaO-SrO, LaO-Sr and La-Sr boundaries replaced by the thin blue lines in Fig. 2). These findings are confirmed by the STEM images reported in [21], in the sense that oxygen atoms are visible at the interface.

III. ELECTRONIC BAND STRUCTURE

Next, we discuss the electronic band structure of the $\text{LaNiO}_2/\text{SrTiO}_3$ heterostructure as a function of the morphology of the interface. Fig. 3 shows the calculated dispersion across the two-dimensional Brillouin zone of the interface and perpendicular to it. We find important changes with respect to the bulk material near the Fermi level depending on the interfacial configuration. These changes can be better understood in relation to the local atomic structure of the interfacial layer. In our calculations, the interfaces are embedded in supercells containing 2 equivalent interfacial Ni_i atoms + 1 “bulk” Ni atoms (surrounded by 1 O_i + 4 O and 4 O atoms respectively, see Fig. 1).

It is instructive to start with the La and Sr interfaces, even if they are the most unlikely configurations according to the overall thermodynamics discussed in the previous section. In fact, the La case can be anticipated to be rather similar to the bulk since the local environment of the interfacial Ni_i is essentially the same. This is confirmed in Fig. 3 where, in addition to the Ni_i - $3d_{x^2-y^2}$ bands crossing the Fermi level, we also observe the self-doping effect due to the La_i - $5d_{z^2}$ ones. These are the main features of the bulk, which are thus preserved at the interface in such a La configuration. The main change is observed at the M point, where two additional bands can be seen near the Fermi level. Their Ni_i orbital character is $3d_{z^2}$ and $3d_{xz/yz}$ along the X - M - Γ line. These features result from the mixing with the La_i - $5d_{xy}$ bands, which now provide an important extra contribution to the La - $5d_{z^2}$ electron self-doping at this interface.

In the case of the Sr interface we observe essentially the same features. The main difference now is the slight overall shift upwards of the bands and, in particular, of their Ni_i - $3d_{z^2}$ character. This is totally in tune with the interfacial hole-doping that results from the $\text{La} \rightarrow \text{Sr}$ local substitution at the interface. This substitution, in addition, has a striking impact on the electron-self doping effect at the interface, which is now surprisingly provided by Ti_i - $3d$ states at Γ (and not by Sr_i - $3d$ ones). Thus, the nature of the metallic character of the system is locally modified by the interfacial configuration.

In the LaO case, more substantial changes are also obtained in the Ni_i bands. First of all, the shift upwards of the originally Ni_i - $3d_{z^2}$ bands is more pronounced. The mixing with the Ni_i - $3d_{x^2-y^2}$ ones is thus enhanced and

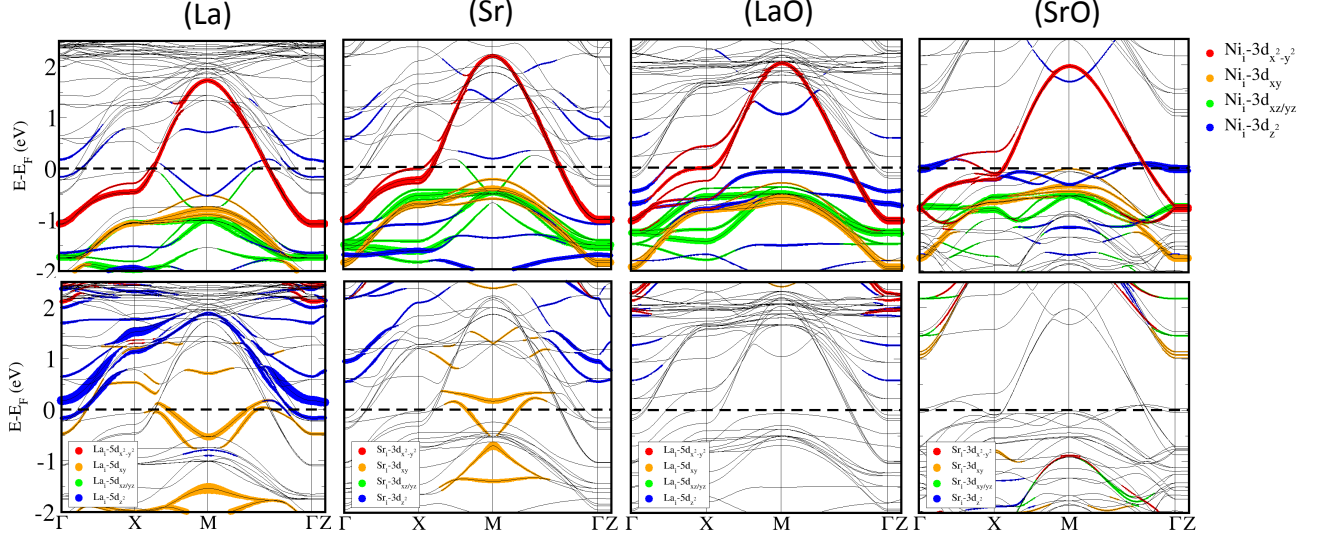


FIG. 3. Band structure of the $\text{LaNiO}_2/\text{SrTiO}_3$ symmetric supercells for different interfacial configurations. The line thickness and the different colors highlight the interfacial contributions according to their atomic-orbital content.

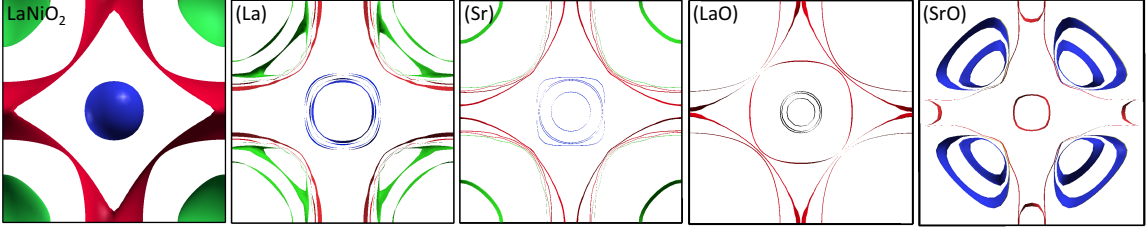


FIG. 4. Top view of the Fermi surface of bulk LaNiO_2 and of the $\text{LaNiO}_2/\text{SrTiO}_3$ heterostructure for the different elementary configurations of the interfacial layer (colors just help to better distinguish the different portions of the Fermi surface).

this is accompanied with an important splitting of the Ni and Ni_i bands along the Γ -X-M path about the Fermi level. These features are in fact associated to avoided band crossings that are best exemplified in bulk fluoronickelates counterparts [29]. The crossing of these bands with the Fermi level is still dominated by the Ni_i - $3d_{x^2-y^2}$ orbitals, even if there is a rather flat Ni_i - $3d_{z^2}$ band right below E_F at the M point. Beyond that, the bands intersecting the Fermi level at Γ have a Ti_i - $3d$ character. Again this is in striking contrast to the bulk and can be associated to the interfacial LaO layer itself.

In the case of SrO, the shift upwards of the Ni_i - $3d_{z^2}$ bands is even more pronounced and the eventual situation is such that only the Ni bands intersect the Fermi level. They now have both $3d_{x^2-y^2}$ and $3d_{z^2}$ orbital contributions. The new bands intersecting the Fermi level are remarkably flat, which is compatible with the formation of a genuine interfacial band localized at the SrO plane. Importantly, there is no electron self-doping effect due to neither Ti - $3d$ nor La - $5d$ contributions in this case. The absence of these contributions is an important qualitative difference compared to the previous configurations and the bulk.

To better understand the interfacial electronic struc-

ture of the LaO and SrO configurations, note that here the interfacial Ni_i is surrounded by an extra oxygen O_i compared to the bulk Ni. This oxygen will tend to take one electron from Ti_i and the other from Ni_i . Thus, the Ni_i - O_i bond will have an important contribution from the Ni - $3d_{z^2}$ orbitals. Taking into account the rather asymmetric arrangement of the Ni_i environment, this can be expected to yield both bondings and backbondings. In fact, in both LaO and SrO configurations, the flat Ni_i - $3d_{z^2}$ band can be associated to such bondings while the empty parabolic band bent upwards with Ni_i - $3d_{z^2}$ character at M can be associated to the backbondings. The Ni_i will thus tend to feature a nominal Ni_i^{2+} oxidation state in the LaO case (where it is surrounded by 8 La) and $\text{Ni}_i^{2.5+}$ in SrO (where it has 4 La and 4 Sr nearby, the latter providing an extra 0.5 hole doping). The extra electrons given by the Ni_i will come from the $3d_{x^2-y^2}$ orbitals, as usual, and from the $3d_{z^2}$ ones via the interfacial oxygen O_i . This explains the shift upwards of the Ni_i - $3d_{z^2}$ bands up to the Fermi level. At the same time, this naturally yields a reduced splitting between Ni- $3d$ and O- $2p$ levels (i.e. charge-transfer energies) compared to the bulk. This reduction is such that even a non-negligible O_i - $2p$ contribution to density of states eventually emerges

at the Fermi energy in the SrO case. Thus, in some sense, these interfacial configurations locally bridge the ‘charge-transfer vs Mott insulator’ gap between bulk cuprates and nickelates [10, 30].

The corresponding Fermi surfaces are shown in Fig. 4. The La, Sr, and LaO configurations yield a sort of direct 2D version of LaNiO₂ Fermi surface. However, the initial electron pockets at Γ (La-5d in the La case as in the bulk) are dominated by Ti-3d orbitals in Sr and LaO, and disappear in SrO. The La and Sr interfaces produce additional pockets at M due to Ni-3d contributions mixed with La-5d and Sr-3d respectively. Most importantly, in the SrO case the initial La-5d pockets at Γ disappear and there appears a series of extra pockets along the Γ - M path. These new pockets are associated to a flat Ni-3d_{z²} band, which is the most distinct feature of the SrO interfacial configuration.

IV. CONCLUSIONS

Infinite-layer nickelate thin films offer an intriguing new platform for unconventional high-temperature superconductivity, with important analogies and differences with respect to the classic case of cuprates. Our work clarifies the specific fundamental features that emerge at the interface and in the ultrathin limit of these systems. To illustrate these features, we have performed a detailed analysis of the reference LaNiO₂/SrTiO₃ heterostructure. The fragile stability of the infinite-layer nickelates in the bulk is found to have a peculiar impact on the energetics of the elementary interfaces. Thus, while the direct growth of epitaxial films is expected to yield LaO as the most stable interfacial configuration, their two-step synthesis via perovskite precursors is found to be compatible with both SrO and Sr interfacial layers too. This has important consequences for the overall electronic band structure that is eventually realized in these films. These can be linked to the local environ-

ment of the interfacial Ni atoms. The most ‘bulk-like’ boundary layer corresponds to the La interfacial configuration, which in fact preserves the main band-structure features of the bulk. The interfacial La \rightarrow Sr replacement, however, produces a striking change in the nature of the metallic character of the system, as the extra La-5d contribution becomes Ti-3d at the interface. Thus, the Kondo physics that emerges due to the coupling between the La-5d and Ni-3d electrons in the bulk [31–33] is lost at the interface. The LaO configuration, in addition, implies an enhanced mix of the Ni-3d_{x²-y²} and Ni-3d_{z²} orbitals near the Fermi level. While this has been argued to be detrimental for superconductivity in cuprates [34], the interfacial Ni-3d_{z²} bands display a remarkable flattening that, by analogy to twisted bilayer graphene and graphite interfaces for example [35, 36], could result into an additional superconducting instability. The SrO interface gives rise to the most dramatic changes. In this case the low-energy physics in the ultrathin limit is in fact entirely determined by Ni-3d electrons, with the original Ni-3d_{x²-y²} features now supplemented by the interfacial Ni-3d_{z²} flat bands exclusively. This changes qualitatively the picture for the subsequent emergence of superconductivity, as the presence of these flat bands need to be fully considered. In particular, even if correlations may stay moderate in the bulk [14], they could dominate the low-energy physics at the interface. Thus, our findings are expected to motivate new perspectives for further theoretical and experimental work on infinite-layer nickelates.

Note added.— After the completion of this work, there appeared a related preprint restricted to the La interfacial configuration reporting complementary results [37].

Acknowledgments. The authors are grateful to V. Olevano and X. Blase for insightful discussions. F.B. acknowledges the Visiting Scientist Program of the Centre de Physique Theorique de Grenoble-Alpes (CPTGA) for financial support.

-
- [1] M. A. Hayward, M. A. Green, M. J. Rosseinsky, and J. Sloan, *J. Am. Chem. Soc.* **121**, 8843 (1999).
 - [2] V. I. Anisimov, D. Bukhvalov, and T. M. Rice, *Phys. Rev. B* **59**, 7901 (1999).
 - [3] K.-W. Lee and W. E. Pickett, *Phys. Rev. B* **70**, 165109 (2004).
 - [4] M. Crespin, O. Isnard, F. Dubois, J. Choisnet, and P. Odier, *Journal of Solid State Chemistry* **178**, 1326 (2005).
 - [5] J. Zhang, A. S. Botana, J. W. Freeland, D. Phelan, H. Zheng, V. Pardo, M. R. Norman, and J. F. Mitchell, *Nature Phys.* **13**, 864 (2017).
 - [6] A. S. Botana, V. Pardo, and M. R. Norman, *Phys. Rev. Materials* **1**, 021801 (2017).
 - [7] D. Li, K. Lee, B. Y. Wang, M. Osada, S. Crossley, H. R. Lee, Y. Cui, Y. Hikita, and H. Y. Hwang, *Nature* **572**, 624 (2019).
 - [8] X. Zhou, Z. Feng, P. Qin, H. Yan, S. Hu, H. Guo, X. Wang, H. Wu, X. Zhang, H. Chen, X. Qiu, and Z. Liu, [arXiv:1911.04662](#).
 - [9] Q. Li, C. He, J. Si, X. Zhu, Y. Zhang, and H.-H. Wen, [arXiv:1911.02420](#).
 - [10] A. S. Botana and M. R. Norman, *Phys. Rev. X* **10**, 011024 (2020).
 - [11] H. Sakakibara, H. Usui, K. Suzuki, T. Kotani, H. Aoki, and K. Kuroki, [arXiv:1909.00060](#).
 - [12] X. Wu, D. D. Sante, T. Schwemmer, W. Hanke, H. Y. Hwang, S. Raghu, and R. Thomale, [arXiv:1909.03015](#).
 - [13] F. Bernardini, V. Olevano, and A. Cano, *Phys. Rev. Research* **2**, 013219 (2020).
 - [14] V. Olevano, F. Bernardini, X. Blase, and A. Cano, [arXiv:2001.09194](#).
 - [15] G. Kresse and J. Furthmüller, *Computational Materials Science* **6**, 15 (1996).

- [16] J. P. Perdew, K. Burke, and M. Ernzerhof, *Phys. Rev. Lett.* **77**, 3865 (1996).
- [17] G. Kresse and D. Joubert, *Phys. Rev. B* **59**, 1758 (1999).
- [18] P. Blaha, K. Schwarz, G. Madsen, D. Kvasnicka, J. Luitz, R. Laskowski, F. Tran, and L. D. Marks, WIEN2k, An Augmented Plane Wave + Local Orbitals Program for Calculating Crystal Properties (Karlheinz Schwarz, Techn. Universität Wien, Austria), 2018. ISBN 3-9501031-1-2.
- [19] J. P. Perdew and A. Zunger, *Phys. Rev. B* **23**, 5048 (1981).
- [20] L. Si, W. Xiao, J. Kaufmann, J. M. Tomczak, Y. Lu, Z. Zhong, and K. Held, [arXiv:1911.06917](#).
- [21] K. Lee, B. H. Goodge, D. Li, M. Osada, B. Y. Wang, Y. Cui, L. F. Kourkoutis, and H. Y. Hwang, [arXiv:2002.07749](#).
- [22] E. Heifets, S. Piskunov, E. A. Kotomin, Y. F. Zhukovskii, and D. E. Ellis, *Phys. Rev. B* **75**, 115417 (2007).
- [23] K. Szot and W. Speier, *Phys. Rev. B* **60**, 5909 (1999).
- [24] V. Vonk, M. Huijben, K. J. I. Driessen, P. Tinnemans, A. Brinkman, S. Harkema, and H. Graafsma, *Phys. Rev. B* **75**, 235417 (2007).
- [25] R. Pentcheva and W. E. Pickett, *Phys. Rev. B* **78**, 205106 (2008).
- [26] G.-X. Qian, R. M. Martin, and D. J. Chadi, *Phys. Rev. B* **38**, 7649 (1988).
- [27] N. Chetty and R. M. Martin, *Phys. Rev. B* **45**, 6089 (1992).
- [28] C. G. Van de Walle, D. B. Laks, G. F. Neumark, and S. T. Pantelides, *Phys. Rev. B* **47**, 9425 (1993).
- [29] F. Bernardini, V. Olevano, X. Blase, and A. Cano, [arXiv:1911.11788](#).
- [30] M. Jiang, M. Berciu, and G. A. Sawatzky, [arXiv:1909.02557](#).
- [31] G.-M. Zhang, Y.-f. Yang, and F.-C. Zhang, *Phys. Rev. B* **101**, 020501 (2020).
- [32] Y.-H. Zhang and A. Vishwanath, [arXiv:1909.12865](#).
- [33] M. Hepting *et al.*, [arXiv:1909.02678](#).
- [34] H. Sakakibara, H. Usui, K. Kuroki, R. Arita, and H. Aoki, *Phys. Rev. B* **85**, 064501 (2012).
- [35] N. B. Kopnin, T. T. Heikkilä, and G. E. Volovik, *Phys. Rev. B* **83**, 220503 (2011).
- [36] See e.g. G. E. Volovik, and the references therein., [arXiv:1803.08799](#).
- [37] B. Geisler and R. Pentcheva, [arXiv:2001.03762](#).

SUPPLEMENTAL MATERIAL

Here, we detail the relative stability of the different interfacial configurations of the relevant heterostructures and the estimate of the chemical potentials. We consider both two step-process followed in [7] and the direct formation of the heterostructure as in [8].

A. $\text{LaNiO}_3/\text{SrTiO}_3$ heterostructure

The elementary interfaces of the perovskite $\text{LaNiO}_3/\text{SrTiO}_3$ heterostructure reduce to either LaO or SrO configurations. Their energy difference can be written as

$$\Delta E_{\text{interface}}^{\text{SrO-LaO}} = \frac{1}{2} \left(E_{\text{tot}}^{(\text{SrO})} - E_{\text{tot}}^{(\text{LaO})} \right) + E_{\text{tot}}^{\text{La}} - E_{\text{tot}}^{\text{Sr}} + \Delta\mu_{\text{La}} - \Delta\mu_{\text{Sr}}, \quad (3)$$

where the total energies are associated to the corresponding supercells. According to Table II, we find that the LaO interface will be energetically favored over the SrO one if $\Delta\mu_{\text{La}} - \Delta\mu_{\text{Sr}} > -2.35$ eV and *vice versa*. This corresponds to the horizontal thick line in blue in Fig. 2.

The actual interval of allowed values of the difference $\Delta\mu_{\text{La}} - \Delta\mu_{\text{Sr}}$ is determined by the minimum and maximum values of the chemical potentials $\Delta\mu_{\text{La}}$ and $\Delta\mu_{\text{Sr}}$ that are compatible with the overall thermodynamics in equilibrium. These are related to $\Delta\mu_{\text{O}}$ as follows.

The existence of bulk LaNiO_3 requires

$$\min \Delta\mu_{\text{La}} = \Delta E_f^{\text{LaNiO}_3} - 3\Delta\mu_{\text{O}}, \quad (4)$$

$$\max \Delta\mu_{\text{La}} = \Delta E_f^{\text{LaNiO}_3} - \min \Delta\mu_{\text{Ni}} - 3\Delta\mu_{\text{O}}. \quad (5)$$

Here we took into account that $\max \Delta\mu_{\text{Ni}} = 0$ in Eq. (4). On the other hand, $\min \Delta\mu_{\text{Ni}}$ must be such that LaNiO_3 does not decompose into La_2O_3 , free O and metallic Ni ($E_f^{\text{LaNiO}_3} < \frac{1}{2}\Delta E_f^{\text{La}_2\text{O}_3} + \frac{3}{2}\Delta\mu_{\text{O}} + \Delta\mu_{\text{Ni}}$) so that

$$\min \Delta\mu_{\text{Ni}} = E_f^{\text{LaNiO}_3} - \frac{1}{2}\Delta E_f^{\text{La}_2\text{O}_3} - \frac{3}{2}\Delta\mu_{\text{O}}. \quad (6)$$

The minimum value of $\Delta\mu_{\text{Sr}}$ must be $\min \Delta\mu_{\text{Sr}} = \Delta E_f^{\text{SrTiO}_3} - \max \Delta\mu_{\text{Ti}} - 3\Delta\mu_{\text{O}}$ according the equilibrium condition for SrTiO_3 . Taking into account that the formation of TiO_2 must be unfavorable (that is, $\max \Delta\mu_{\text{Ti}} = \Delta E_f^{\text{TiO}_2} - 2\Delta\mu_{\text{O}}$) we then have

$$\min \Delta\mu_{\text{Sr}} = \Delta E_f^{\text{SrTiO}_3} - \Delta E_f^{\text{TiO}_2} - \Delta\mu_{\text{O}}. \quad (7)$$

	ΔE_f (eV)	E_{tot} (eV)	a (Å)	c (Å)	Space group
LaNiO ₃	-12.27	-35.90	3.829	3.829	$P4/mmm$
LaNiO ₂	-9.77	-28.96	3.936	3.393	$P4/mmm$
LaNiO	-5.42	-20.18	3.584	3.842	$P4/mmm$
La ₂ O ₃	-18.78	-41.84	3.937	6.181	$P6_3/mmc$
NiO	-1.48	-11.36	4.151	4.151	$Fm\bar{3}m$
La	-	-4.88	3.767	12.129	$P6_3/mmc$
Ni	-	-5.44	3.499	3.499	$Fm\bar{3}m$
SrTiO ₃	-17.35	-40.11	3.940	3.940	$Pm\bar{3}m$
SrO	-5.99	-12.06	5.203	5.203	$Fm\bar{3}m$
TiO ₂	-9.17	-25.87	4.160	8.579	$I4_1/amd$
Sr	-	-1.64	6.038	6.038	$Fm\bar{3}m$
Ti	-	-7.84	2.939	4.640	$P6_3/mmc$
CaH ₂ O ₂	-10.55	-28.10	3.618	4.913	$P\bar{3}m1$
CaH ₂	-1.69	-10.38	*	6.760	$Pnma$

TABLE II. Formation energy and structural parameters of the different compounds used to determine the chemical potentials that define the interface energy according to Eq. (1). The formation energy of LaNiO₂, for example, is defined as $\Delta E_f^{\text{LaNiO}_2} = E_{\text{tot}}^{\text{LaNiO}_2} - E_{\text{tot}}^{\text{La}} - E_{\text{tot}}^{\text{Ni}} - E_{\text{tot}}^{\text{O}_2}$, and a similar definition applies for the rest of compounds. *In the case of the orthorhombic CaH₂ the lattice parameters perpendicular to the c axis are $a = 5.892$ Å and $b = 3.568$ Å.

The maximum value of $\Delta\mu_{\text{Sr}}$, on the other hand, is determined the condition of unfavourable formation of SrO,

$$\max \Delta\mu_{\text{Sr}} = \Delta E_f^{\text{SrO}} - \Delta\mu_{\text{O}}. \quad (8)$$

Regarding $\Delta\mu_{\text{O}}$ itself, this potential should be high enough so that LaNiO₃ does not decompose into LaNiO₂. This implies $\Delta E_f^{\text{LaNiO}_3} < \Delta E_f^{\text{LaNiO}_2} + \Delta\mu_{\text{O}}$ which, according to the energies listed in Table II, further means that -2.50 eV $< \Delta\mu_{\text{O}}$. This is marked by the dashed yellow line in Fig. 2. At the same time, LaNiO₃ should also be stable with respect its decomposition into La₂O₃ and NiO. This, however, is ensured by the fact that the inequality $\Delta E_f^{\text{LaNiO}_3} < \frac{1}{2}\Delta E_f^{\text{La}_2\text{O}_3} + \Delta E_f^{\text{NiO}} + \frac{1}{2}\Delta\mu_{\text{O}}$ holds whenever -2.50 eV $< \Delta\mu_{\text{O}}$.

We then note that Eq. (5) must be used with caution since, according to Table II, one obtains a positive value of $\max \Delta\mu_{\text{La}}$ for $\Delta\mu_{\text{O}} > -1.92$ eV. This is incompatible with the fact that the chemical potentials are such that $\Delta\mu_{\text{X}} < 0$. Consequently, in the O-rich situation in which $\Delta\mu_{\text{O}} > -1.92$ eV we can safely put $\max \Delta\mu_{\text{La}} = 0$.

Thus, subtracting Eq. (8) from Eq. (4) we obtain the minimum value for the difference $\Delta\mu_{\text{La}} - \Delta\mu_{\text{Sr}}$ as

$$\min(\Delta\mu_{\text{La}} - \Delta\mu_{\text{Sr}}) = \Delta E_f^{\text{LaNiO}_3} - \Delta E_f^{\text{SrO}} - 2\Delta\mu_{\text{O}}, \quad (9)$$

while subtracting Eq. (7) from Eq. (5) we obtain its maximum value

$$\max(\Delta\mu_{\text{La}} - \Delta\mu_{\text{Sr}}) = \begin{cases} \Delta E_f^{\text{LaNiO}_3} - \Delta E_f^{\text{SrTiO}_3} + \Delta E_f^{\text{TiO}_2} - 2\Delta\mu_{\text{O}} & (\Delta\mu_{\text{O}} < -1.92 \text{ eV, O-poor}), \\ \frac{1}{2}\Delta E_f^{\text{La}_2\text{O}_3} - \Delta E_f^{\text{SrTiO}_3} + \Delta E_f^{\text{TiO}_2} - \frac{1}{2}\Delta\mu_{\text{O}} & (\Delta\mu_{\text{O}} > -1.92 \text{ eV, O-rich}). \end{cases} \quad (10)$$

Eqs. (9) and (10) give rise to the yellow region in Fig. 2, which is determined according to the values listed in Table II. We find, in particular,

$$-1.28 \text{ eV} < \Delta\mu_{\text{La}} - \Delta\mu_{\text{Sr}} < +0.91 \text{ eV} \quad (\Delta\mu_{\text{O}} = -2.5 \text{ eV}), \quad (11)$$

$$-6.28 \text{ eV} < \Delta\mu_{\text{La}} - \Delta\mu_{\text{Sr}} < -1.21 \text{ eV} \quad (\Delta\mu_{\text{O}} = 0 \text{ eV}). \quad (12)$$

B. Topotactic reduction

In [7] the LaNiO₃/SrTiO₃ sample was vacuum-sealed together with—but not in direct contact to—CaH₂ powder for the topotactic reaction. Then a gas-phase reaction is activated upon heating in which oxygen is removed from LaNiO₃ and incorporated the powder yielding CaH₂O₂. In this reaction $\Delta\mu_{\text{O}}$ is lowered so that LaNiO₃ is forced to loose oxygen atoms (i.e. below -2.5 eV). Its eventual value have to be such that

$$\Delta E_f^{\text{CaH}_2\text{O}_2} < \Delta E_f^{\text{CaH}_2} + 2\Delta\mu_{\text{O}}. \quad (13)$$

According to Table II that means $\Delta\mu_{\text{O}} > -4.43$ eV, which is marked by the dashed blue line in Fig. 2. We note that -4.43 eV is just slightly below the minimum value of $\Delta\mu_{\text{O}}$ in LaNiO_2 (see below), which means that a more reducing environment would produce LaNiO instead of LaNiO_2 out of LaNiO_3 .

Regarding the possible reduction of SrTiO_3 to SrTiO_2 , for this to happen the O chemical potential has to satisfy the condition $\Delta E_f^{\text{SrTiO}_3} > \Delta E_f^{\text{SrTiO}_2} + \Delta\mu_{\text{O}}$ which, according to the energies listed in Table II, further means that $\Delta\mu_{\text{O}} < -5.65$ eV. This, however, is incompatible with the limit set by the topotactic reduction reaction (-4.4 eV $< \Delta\mu_{\text{O}}$). Thus, we conclude that the topotactic reduction can certainly remove O from LaNiO_3 but will not be able to transform SrTiO_3 into SrTiO_2 .

C. $\text{LaNiO}_2/\text{SrTiO}_3$ heterostructure

The energy difference between the La and LaO interfacial configurations reads

$$\Delta E_{\text{interface}}^{\text{La-LaO}} = \frac{1}{2} (E_{\text{tot}}^{(\text{La})} - E_{\text{tot}}^{(\text{LaO})} + E_{\text{tot}}^{\text{O}_2}) + \Delta\mu_{\text{O}}. \quad (14)$$

Accordingly, the LaO interface will be favored over the La one if $\Delta\mu_{\text{O}} > -4.38$ eV (and vice versa). Similarly, we find that the SrO interface will be favored over the Sr one if $\Delta\mu_{\text{O}} > -3.67$ eV. The boundaries defined by these relative stabilities are indicated by the thick vertical lines in blue in Fig. 2, and apply for both the topotactic reduction and the direct growth of the $\text{LaNiO}_2/\text{SrTiO}_3$ heterostructure.

Consider now the formation-energy difference between the SrO and LaO, Sr and LaO, and Sr and La interfaces:

$$\Delta E_{\text{interface}}^{\text{SrO-LaO}} = \frac{1}{2} (E_{\text{tot}}^{(\text{SrO})} - E_{\text{tot}}^{(\text{LaO})}) + E_{\text{tot}}^{\text{La}} - E_{\text{tot}}^{\text{Sr}} + \Delta\mu_{\text{La}} - \Delta\mu_{\text{Sr}}, \quad (15)$$

$$\Delta E_{\text{interface}}^{\text{Sr-LaO}} = \frac{1}{2} (E_{\text{tot}}^{(\text{Sr})} - E_{\text{tot}}^{(\text{LaO})} + E_{\text{tot}}^{\text{O}_2}) + E_{\text{tot}}^{\text{La}} - E_{\text{tot}}^{\text{Sr}} + \Delta\mu_{\text{La}} - \Delta\mu_{\text{Sr}} + \Delta\mu_{\text{O}}. \quad (16)$$

$$\Delta E_{\text{interface}}^{\text{Sr-La}} = \frac{1}{2} (E_{\text{tot}}^{(\text{Sr})} - E_{\text{tot}}^{(\text{La})}) + E_{\text{tot}}^{\text{La}} - E_{\text{tot}}^{\text{Sr}} + \Delta\mu_{\text{La}} - \Delta\mu_{\text{Sr}}, \quad (17)$$

According to the computed values of the total energies (Tables I and II), we find that the LaO interface is energetically favored with respect to the SrO one if $\Delta\mu_{\text{La}} - \Delta\mu_{\text{Sr}} > -1.54$ eV. The LaO configuration is additionally favored over the Sr one if $\Delta\mu_{\text{La}} - \Delta\mu_{\text{Sr}} + \Delta\mu_{\text{O}} > -5.21$ eV. Finally, we find that the La interface is energetically favored with respect to the Sr one if $\Delta\mu_{\text{La}} - \Delta\mu_{\text{Sr}} > -0.83$ eV. These considerations are relevant for the direct growth of the $\text{LaNiO}_2/\text{SrTiO}_3$ heterostructure only (since they imply $\text{La} \leftrightarrow \text{Sr}$ replacements that, in principle, cannot be obtained by means of the topotactic reduction of the perovskite), and are indicated by thin blue lines in Fig. 2.

In terms of $\Delta\mu_{\text{O}}$, the realization of the nickelate in its infinite-layer phase requires the following. On one hand, LaNiO_2 has to be more stable than LaNiO_3 . That is, $\Delta E_f^{\text{LaNiO}_2} < \Delta E_f^{\text{LaNiO}_3} - \Delta\mu_{\text{O}}$. At the same time, LaNiO_2 must be more stable than $\text{LaNiO} + \text{O}$. That is, $\Delta E_f^{\text{LaNiO}_2} < E_f^{\text{LaNiO}} + \Delta\mu_{\text{O}}$. Taken together, these two conditions tell us that

$$-4.35 \text{ eV} < \Delta\mu_{\text{O}} < -2.50 \text{ eV} \quad (18)$$

according to the formation energies listed in Table II. The limits of this interval correspond to the dashed lines in Fig. 2. We note that NiO is never stable within such a $\Delta\mu_{\text{O}}$ interval, so that $\Delta\mu_{\text{Ni}}$ can reach 0 (*i.e.* $\max \Delta\mu_{\text{Ni}} = 0$). Further, the potentials need to be such that

$$\min \Delta\mu_{\text{La}} = \Delta E_f^{\text{LaNiO}_2} - 2\Delta\mu_{\text{O}}, \quad (19)$$

$$\max \Delta\mu_{\text{Sr}} = \Delta E_f^{\text{SrO}} - \Delta\mu_{\text{O}}, \quad (20)$$

By subtracting these equations and using Table II we find that

$$\min[\Delta\mu_{\text{La}} - \Delta\mu_{\text{Sr}}] + \Delta\mu_{\text{O}} = -3.78 \text{ eV}. \quad (21)$$

This further defines the blue region in Fig. 2.